

Capacity-Approaching Polar Codes with Long Codewords and Successive Cancellation Decoding Based on Improved Gaussian Approximation

Hideki Ochiai, *Senior Member, IEEE*, Patrick Mitran, *Senior Member, IEEE*, and H. Vincent Poor, *Fellow, IEEE*

Abstract

This paper focuses on an improved Gaussian approximation (GA) based construction of polar codes with successive cancellation (SC) decoding over an additive white Gaussian noise (AWGN) channel. Arıkan has proven that polar codes with low-complexity SC decoder can approach the channel capacity of an arbitrary symmetric binary-input discrete memoryless channel, provided that the code length is chosen large enough. Nevertheless, how to construct such codes over an AWGN channel with low computational effort has been an open problem. Compared to density evolution, the GA is known as a low complexity yet powerful technique that traces the evolution of the mean log likelihood ratio (LLR) value by iterating a nonlinear function. Therefore, its high-precision numerical evaluation is critical as the code length increases. In this work, by analyzing the asymptotic behavior of this nonlinear function, we propose an improved GA approach that makes an accurate trace of mean LLR evolution feasible. With this improved GA, through numerical analysis and simulations with code lengths up to $N = 2^{18}$, we explicitly demonstrate that various code-rate polar codes with long codeword and capacity approaching behavior can be easily designed.

Index Terms

Block error rate, code construction, density evolution, Gaussian approximation, polar codes.

H. Ochiai is with the Department of Electrical and Computer Engineering, Yokohama National University, Yokohama, Japan. email: hideki@ynu.ac.jp

P. Mitran is with the Department of Electrical and Computer Engineering, University of Waterloo, ON, Canada. email:mitran@uwaterloo.ca

H. V. Poor is with the Department of Electrical Engineering, Princeton University, Princeton, NJ. email: poor@princeton.edu

This work was supported in part by the Japan Society for the Promotion of Science (JSPS) through the Grants-in-Aid for Scientific Research (KAKENHI) under Grant JP16KK0145, in part by the Natural Sciences and Engineering Research Council of Canada (NSERC), and in part by the U.S. National Science Foundation under Grant CCF-1908308.

I. INTRODUCTION

Polar codes, introduced by Arikan [1], have the salient property that they can achieve channel capacity by low-complexity successive cancellation (SC) decoding. In order to approach capacity over a practical additive white Gaussian noise (AWGN) channel by SC decoding, not only must the polar code length be large, but the code structure must also be properly designed. A key difficulty of polar code design over binary-input AWGN channels lies in the fact that the optimal polar code that yields the lowest block error rate (BLER) by SC decoding may have different code structure depending on the specific channel signal-to-noise power ratio (SNR). Therefore, practical code design should be able to predict its BLER performance for given operating SNR and code rate.

In the framework of polar codes, code construction is equivalent to the selection of information bit locations, collectively referred to as the *information set* [1]. These are chosen from among all the input bits to the rate-1 polar encoder. Several approaches for polar code construction, i.e., algorithms for information set selection, have been developed in the literature for an AWGN channel. Mori and Tanaka [2] proposed the use of density evolution (DE), originally developed for the design of irregular low-density parity-check (LDPC) codes by Richardson *et al.* in [3]. Since memory and computation requirements for direct tracing of density grow exponentially with code length, Tal and Vardy developed a tractable approach that manages the memory requirements by efficiently merging the density [4] through quantization at the cost of a loss in channel capacity. The resulting algorithms (with channel upgrading and degrading due to quantization) were shown to provide rigorous upper and lower bounds to the achievable performance, and their tightness depends on the number of quantization levels μ . Upon merging the density, the sorting of likelihood ratios with memory size of order $O(\mu^2)$ is required, and the overall complexity of this is of order $O(N\mu^2 \log \mu)$ for polar codes with codeword length N [4]. In order to tighten the bounds, one should increase μ without sacrificing numerical accuracy when calculating the loss in channel capacity. This makes the algorithm computationally challenging, especially for the design of polar codes with large block lengths under various operating SNR. Other constructions include reduced complexity DE based on the sub-optimal min-sum algorithm [5], which still imposes a memory requirement that grows exponentially as the codeword length increases.

Meanwhile, for design and analysis of LDPC codes, Chung *et al.* proposed the use of a Gaussian approximation (GA) [6]. Instead of tracing the exact density of the log likelihood

ratios (LLR), GA only traces the mean value. This becomes a sufficient statistic to characterize the LLR provided that the LLR is assumed to be modeled, for some $\gamma > 0$, as a Gaussian distribution with mean γ and variance 2γ . Since the GA method can be implemented with only a few computations (that involve nonlinear functions), the overall complexity is proportional to the codeword length N . Trifonov [7] demonstrated that the GA can be also used for constructing polar codes with SC decoding. Subsequently, the effectiveness of the GA for polar code construction has been confirmed in [8], [9]. Furthermore, in [9], [10], the use of the Bhattacharyya parameter [1] for information set selection, which is strictly valid only for the case of binary erasure channels, has been shown by simulation to be effective provided that the operating SNR parameter is appropriately chosen by an empirical approach.

In order for polar codes with SC decoding to outperform LDPC codes, it is known that the code length should be much larger than that of LDPC codes [11]. In other words, polar codes over an AWGN channel with moderate code length are not competitive with other capacity approaching codes. Since then, the use of other decoding approaches such as belief propagation (BP) decoding has also been studied [12]–[14]. On the other hand, Tal and Vardy showed that successive cancellation *list* (SCL) decoding improves the performance, and furthermore, the application of error detection codes such as cyclic redundancy-check (CRC) codes in combination with SCL decoding is shown to outperform other competitive codes [15]. Subsequently, most studies on polar codes target moderate block-length codes assuming more sophisticated decoding. As a consequence, studies for polar code construction have also pursued decoding specific designs such as those proposed in [16] and [17].

Here, we recall that a major advantage of polar codes as proposed by Arikan [1] is its simplicity of encoding and SC decoding with its capacity achieving performance. The only issue is that the code length should be much larger compared to LDPC codes [11] for the same or better target performance. Therefore, this paper focuses on constructing polar codes for SC decoding with very large code lengths (i.e., larger than 10^5 bits) and evaluating their performance over a practical AWGN channel based on GA as a low-complexity design approach compared to the original DE. Furthermore, the assumption of GA enables us to derive an estimate of the BLER without resorting to time-consuming simulations. In this work, we first elucidate the limitation of the conventional GA in its mean LLR estimation process, especially as the code length increases. It turns out that the straightforward implementation of conventional GA fails to construct good polar codes with capacity approaching behavior at large block length (as will be illustrated in Fig. 5

in Section V-B). This stems from the fact that the dynamic range of the LLR values increases exponentially with code length, and thus the conventional approach cannot accurately trace the evolution of mean LLR values. We then propose a solution to this numerical issue by carefully studying the behavior of specific functions involved in GA. With this proposed approach, which we refer to as an *improved GA*, we can easily estimate the performance of polar codes with SC decoding for long codes with low complexity. We then demonstrate simulation results with block lengths up to $N = 2^{18}$ and show that the results match well with the estimated BLER results obtained by the analysis using the improved GA. A similar but empirical modification that improves the performance of GA has been proposed by Ha *et al.* [18], and our analytical studies also serve as a justification of their approach.

Furthermore, we investigate a second construction based on the flipping probability of an LLR. Similar to the case of the GA method, this approach can estimate the BLER without simulation. By tracing the flipping probability instead of its mean value, it is still possible to construct codes with large length, even though numerical results show its sub-optimality over the improved GA as the code length increases. Note that both the GA and LLR flipping approaches are based on the assumption that the LLR can be modeled as Gaussian. Since this is an approximation, its accuracy is evaluated by comparing the estimated performance based on this approximation with that obtained by simulation.

The major contributions of this paper are summarized as follows:

- The GA method should trace the evolution of the mean LLR value through nonlinear transformation. Based on the log-domain analysis of this transformation process, a new algorithm with closed-form expressions that can trace the evolution with improved accuracy over an AWGN channel is developed.
- How to design the key SNR parameter in the code construction algorithm is discussed based on the estimated BLER. Using this measure, the capacity-approaching behavior of polar codes with various code rates is demonstrated with low-complexity SC decoding.
- The effectiveness of the proposed GA is investigated through comparison with the other construction alternatives of the same complexity order by Monte-Carlo simulation with block-lengths as large as $N = 2^{18} = 262\,144$.

We note that the use of codeword lengths of 10^5 or more has been considered in several applications such as high-speed optical communications [19], optical recording systems [20], and flash memories [21], where product codes are often adopted due to practical constraints on

encoding/decoding complexity associated with long codeword lengths. Therefore, we expect that polar codes could be an alternative solution in the future as polar codes with SC decoding can be implemented with low encoding/decoding complexity, provided that good polar codes with such long codeword lengths can be designed with reasonable complexity.

This paper is organized as follows. Section II introduces notations associated with polar codes and decoding used throughout this work. The construction based on the conventional GA method is reviewed and the proposed calculation approach is presented in Section III. As an alternative and tractable approach to the GA method, a construction based on LLR flipping probability is described in Section IV. Numerical examples are given in Section V, where the capacity-approaching behavior based on the construction using the improved GA is demonstrated, together with comprehensive comparison with the other approaches. Finally, Section VI concludes this work.

II. POLAR CODES AND SUCCESSIVE CANCELLATION DECODING

A. Polar Code

Let $\mathbf{u} = (u_0, u_1, \dots, u_{N-1}) \in \mathbb{F}_2^N$ denote a binary input vector of length N . Let $\mathbf{G}_N \in \mathbb{F}_2^{N \times N}$ denote a generator matrix formulated as

$$\mathbf{G}_N = \mathbf{G}_2^{\otimes n}, \quad \mathbf{G}_2 = \begin{pmatrix} 1 & 0 \\ 1 & 1 \end{pmatrix}, \quad (1)$$

where $n = \log_2 N$ and $\mathbf{A}^{\otimes n} = \mathbf{A} \otimes \mathbf{A}^{\otimes (n-1)}$ is the n th Kronecker power of matrix \mathbf{A} with $\mathbf{A}^{\otimes 0} = (1)$ [1]. The corresponding output $\mathbf{x} = (x_0, x_1, \dots, x_{N-1}) \in \mathbb{F}_2^N$ is expressed as

$$\mathbf{x} = \mathbf{u} \mathbf{B}_N \mathbf{G}_N, \quad (2)$$

where $\mathbf{B}_N \in \mathbb{F}_2^{N \times N}$ is the $N \times N$ bit reversal permutation matrix [1] which guarantees that SC decoding is performed in the bit reversal order of the binary channel index.

We assume BPSK modulation over an AWGN channel, i.e., the transmitted symbol $s_i \in \mathbb{R}$, $i = 0, 1, \dots, N-1$, is given by

$$s_i = \sqrt{E_s}(1 - 2x_i), \quad (3)$$

with E_s representing the symbol energy, and the received symbol $y_i \in \mathbb{R}$ is

$$y_i = s_i + z_i, \quad (4)$$

where $z_i \sim \mathcal{N}(0, N_0/2)$, i.e., z_i is a real-valued Gaussian random variable with zero mean and variance $N_0/2$. We denote the received signal vector of length $N = 2^n$ as $\mathbf{y}_n = (y_0, y_1, \dots, y_{2^n-1})$, and its sub-vector of length 2^m starting from the index i as $\mathbf{y}_m^{(i)} = (y_i, y_{i+1}, \dots, y_{i+2^m-1})$.

B. Successive Cancellation Decoding

Based on SC decoding, given the length- 2^n received symbol observation vector \mathbf{y}_n , each input bit u_i , $i = 0, 1, \dots, N - 1$, is decoded successively based on its corresponding LLR. We use the following short-hand notation for LLR of the i th input bit u_i as

$$L_n^{(i)}(\mathbf{y}_n) = \begin{cases} \log \frac{p(\mathbf{y}_n | u_i=0)}{p(\mathbf{y}_n | u_i=1)}, & i = 0, \\ \log \frac{p(\mathbf{y}_n, \hat{\mathbf{u}}_{i-1} | u_i=0)}{p(\mathbf{y}_n, \hat{\mathbf{u}}_{i-1} | u_i=1)}, & i = 1, 2, \dots, 2^n - 1, \end{cases} \quad (5)$$

where $p(\cdot|\cdot)$ denotes a conditional probability density function and $\hat{\mathbf{u}}_{i-1} = (\hat{u}_0, \hat{u}_1, \dots, \hat{u}_{i-1})$ is the vector containing the estimated bits that have been already determined upon decoding of the i th bit. (The subscript n of $L_n^{(i)}$ reflects the fact that the LLR is calculated based on the observation of 2^n received symbols in addition to the previously estimated input bits.) Note that for simplicity of notation, we will omit the dependence of LLR on the previously estimated bits $\hat{\mathbf{u}}_{i-1}$ in what follows.

Because of the unique structure of polar codes, the above LLRs can be recursively calculated for $k = 1, 2, \dots, n$ with $n = \log_2 N$ and $i = 0, 1, \dots, 2^{k-1} - 1$ as [1], [2]

$$L_k^{(2i)}(\mathbf{y}_k) = L_{k-1}^{(i)}(\mathbf{y}_{k-1}^{(0)}) \boxplus L_{k-1}^{(i)}(\mathbf{y}_{k-1}^{(2^{k-1})}) \quad (6)$$

$$L_k^{(2i+1)}(\mathbf{y}_k) = L_{k-1}^{(i)}(\mathbf{y}_{k-1}^{(2^{k-1})}) + (-1)^{\hat{u}_{2i}} L_{k-1}^{(i)}(\mathbf{y}_{k-1}^{(0)}). \quad (7)$$

Alternatively, by rewriting $L_k^{(2i)} \triangleq L_k^{(2i)}(\mathbf{y}_k)$, $L_{k-1}^{(i)} \triangleq L_{k-1}^{(i)}(\mathbf{y}_{k-1}^{(0)})$, and $L_{k-1}^{(i)'} \triangleq L_{k-1}^{(i)}(\mathbf{y}_{k-1}^{(2^{k-1})})$ for simplicity, we have

$$L_k^{(2i)} = L_{k-1}^{(i)} \boxplus L_{k-1}^{(i)'} \quad (8)$$

$$L_k^{(2i+1)} = L_{k-1}^{(i)'} + (-1)^{\hat{u}_{2i}} L_{k-1}^{(i)}. \quad (9)$$

As noted in [2], (8) corresponds to the LLR calculation associated with a check node, whereas (9) corresponds to that with a variable node (or bit node) in the Tanner graph. The operation \boxplus of LLR is defined as [22]

$$L_a \boxplus L_b = \log \frac{1 + e^{L_a} e^{L_b}}{e^{L_a} + e^{L_b}} = 2 \tanh^{-1} \left(\tanh \left(\frac{L_a}{2} \right) \tanh \left(\frac{L_b}{2} \right) \right). \quad (10)$$

The recursive decoding procedure continues, starting from $k = n$ and until it reaches 1, where the last LLR on the right hand side of (6) and (7), i.e., $L_0^{(0)}(y_i)$, corresponds to the LLR of the channel bit x_i . For an AWGN channel, we have

$$L_0^{(0)}(y_i) = \log \frac{p(y_i | x_i = 0)}{p(y_i | x_i = 1)} = 4 \frac{\sqrt{E_s}}{N_0} y_i, \quad i = 0, 1, \dots, N - 1. \quad (11)$$

C. Polar Code Construction

For polar codes with rate $R = K/N$, K channel indices out of N total indices are selected for information transmission. Let $\mathcal{I} \subset \{0, 1, \dots, N - 1\}$ denote the set of the channel indices selected to be information bits, i.e., the *information set* [1], with its cardinality given by $|\mathcal{I}| = K$. The bits that are not in this set are called *frozen bits* and fixed to known values (usually set as 0). Therefore, polar code construction is equivalent to the selection of a set \mathcal{I} that leads to a good block error rate (BLER) performance.

In this work, we mostly focus on a Gaussian approximation (GA) based design of polar codes. This approach allows us to construct good polar codes with much less complexity than those based on precise calculation using density evolution. We demonstrate that the carefully designed GA will also be able to predict the resulting BLER performance achieved by simulations for a given code with almost negligible computational effort.

III. IMPROVED GAUSSIAN APPROXIMATION

In this section, we first study the conventional GA approach, originally proposed for design and analysis of LDPC codes, and its limitations when applied to the design of polar codes. Then, through careful design of associated metric calculations, we show how to overcome these limitations by an improved GA.

A. Gaussian Approximation

Assume that the all-zero input sequence and thus the all-zero codeword is transmitted. Then, from (3) and (4), $y_i \sim \mathcal{N}(\sqrt{E_s}, N_0/2)$ for all i and thus from (11) we observe that $L_0^{(0)} \triangleq L_0^{(0)}(y_i) \sim \mathcal{N}(\gamma_0, 2\gamma_0)$ with $\gamma_0 = 4E_s/N_0$. When the value E_s/N_0 is used for construction of polar codes, we refer to this value as the *design SNR* [7], [10], denoted by SNR_{des} . Otherwise, E_s/N_0 corresponds to the channel SNR. (Note that the design SNR in this work is not given with respect to the conventional E_b/N_0 where E_b is defined as the energy *per information bit*.)

This is because E_b/N_0 is a function of both E_s/N_0 and the code rate, and thus is not convenient when comparing transmissions of codewords with the same symbol energy but different code rate.) From (8), (9), and (10) with the assumption that the previous bits are correctly estimated (i.e., $\hat{\mathbf{u}}_{i-1} = \mathbf{0}_i$ for a given i , where $\mathbf{0}_m$ denotes the zero vector of length m), we have

$$\tanh\left(\frac{L_k^{(2i)}}{2}\right) = \tanh\left(\frac{L_{k-1}^{(i)}}{2}\right) \tanh\left(\frac{L_{k-1}^{(i)'}}{2}\right), \quad (12)$$

$$L_k^{(2i+1)} = L_{k-1}^{(i)} + L_{k-1}^{(i)'}, \quad (13)$$

for $k = 1, 2, \dots, n$, and $i = 0, 1, \dots, 2^{k-1} - 1$ with $n = \log_2 N$, where both $L_{k-1}^{(i)}$ and $L_{k-1}^{(i)'}$ can be considered as independent and identically distributed (i.i.d.) random variables due to the structure of the polar codes with SC decoding. Under the assumption that the LLRs $L_{k-1}^{(i)}$ and $L_{k-1}^{(i)'}$ follow a $\mathcal{N}(\gamma_{k-1}^{(i)}, 2\gamma_{k-1}^{(i)})$ distribution, the only parameter required to characterize its statistical distribution is its mean. In fact, if this Gaussian assumption holds, since the two LLRs on the right hand side of (13) are statistically independent, it follows from (13) that the output $L_k^{(2i+1)}$ should precisely follow $\mathcal{N}(2\gamma_{k-1}^{(i)}, 4\gamma_{k-1}^{(i)})$, i.e.,

$$\gamma_k^{(2i+1)} = 2\gamma_{k-1}^{(i)}. \quad (14)$$

On the other hand, the transformation (12) changes the statistical distribution of the output $L_k^{(2i)}$ from Gaussian. Nevertheless, Chung *et al.* applied statistical expectation to both sides of (12) to get [6]

$$\begin{aligned} E\left[\tanh\left(\frac{L_k^{(2i)}}{2}\right)\right] &= E\left[\tanh\left(\frac{L_{k-1}^{(i)}}{2}\right)\right] E\left[\tanh\left(\frac{L_{k-1}^{(i)'}}{2}\right)\right] \\ &= \left(E\left[\tanh\left(\frac{L_{k-1}^{(i)}}{2}\right)\right]\right)^2. \end{aligned} \quad (15)$$

Upon calculating (15), let us define the monotonically increasing function $\psi(\gamma) : (0, \infty) \rightarrow (0, 1)$ with respect to the mean γ of the random variable $L \sim \mathcal{N}(\gamma, 2\gamma)$ as

$$\psi(\gamma) \triangleq E\left[\tanh\left(\frac{L}{2}\right)\right] = \int_{-\infty}^{\infty} \tanh\left(\frac{x}{2}\right) \frac{1}{\sqrt{4\pi\gamma}} e^{-\frac{(x-\gamma)^2}{4\gamma}} dx. \quad (16)$$

Now, following [23], let us introduce the short-hand notation for the compound function:

$$\Xi(\gamma) \triangleq \psi^{-1}(\psi^2(\gamma)). \quad (17)$$

Then, we may rewrite (15) as

$$\gamma_k^{(2i)} = \Xi\left(\gamma_{k-1}^{(i)}\right). \quad (18)$$

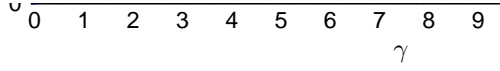


Fig. 1. The mean LLR converting functions $\psi(\gamma)$, $\phi(\gamma)$, and its associated function $\psi^2(\gamma)$. The trajectories demonstrate how the mean value is converted by the equation (17).

Note that the compound function $\Xi(\gamma) : (0, \infty) \rightarrow (0, \infty)$ is monotonically increasing. However, since $\psi(\gamma)$ is strictly increasing in γ with $0 < \psi(\gamma) < 1$, we have $\psi^2(\gamma) < \psi(\gamma)$ and hence $\Xi(\gamma) = \psi^{-1}(\psi^2(\gamma)) < \gamma$. Therefore, for $\gamma > 0$, $\Xi(\gamma)$ is always a value that is strictly smaller than its input γ .

Instead of directly dealing with $\psi(\gamma)$, Chung *et al.* introduce its complement function

$$\phi(\gamma) = 1 - \psi(\gamma). \quad (19)$$

In this case, $\phi(\gamma)$ is a monotonically decreasing function and approaches zero as $\gamma \rightarrow \infty$, and (18) is equivalent to

$$\gamma_k^{(2i)} = \phi^{-1} \left(1 - \left(1 - \phi \left(\gamma_{k-1}^{(i)} \right) \right)^2 \right). \quad (20)$$

Fig. 1 plots the associated functions $\psi(\gamma)$, $\psi^2(\gamma)$, and $\phi(\gamma)$, which are calculated by numerical integration. The trajectories in the figure show how the mean value γ is converted by the transformation of (17), and it is apparent that this transformation always reduces the mean LLR value.

In [6], the following approximation for $\phi(\gamma)$ in (19) was suggested:

$$\phi(\gamma) \approx e^{a\gamma^c + b}, \quad \gamma \leq \Gamma_{\text{th}}, \quad (21)$$

where the constants were numerically determined as $(a, b, c) = (-0.4527, 0.0218, 0.86)$, and the threshold was chosen as $\Gamma_{\text{th}} \approx 10$. For the case of $\gamma > \Gamma_{\text{th}}$, based on the relationship

$$\sqrt{\frac{\pi}{\gamma}} e^{-\frac{\gamma}{4}} \left(1 - \frac{3}{\gamma}\right) < \phi(\gamma) < \sqrt{\frac{\pi}{\gamma}} e^{-\frac{\gamma}{4}} \left(1 + \frac{1}{7\gamma}\right), \quad (22)$$

and since the upper and lower bounds converge as $\gamma \rightarrow \infty$, it was suggested to approximate $\phi(\gamma)$ by the average of the upper and lower bounds in (22), i.e.,

$$\phi(\gamma) \approx \sqrt{\frac{\pi}{\gamma}} e^{-\frac{\gamma}{4}} \left(1 - \frac{10}{7\gamma}\right). \quad (23)$$

For small γ , (21) may not be accurate as $\gamma \rightarrow 0$. Therefore, even if (21) may be sufficient for the moderate size of N as confirmed in [8], [9], the performance degradation may occur for large code length N due to numerical inaccuracy.

There are two numerical computation issues with the above GA approach. The first issue is due to the approximation associated with (21) for a small value of γ , which results in $\lim_{\gamma \rightarrow 0} \phi(\gamma) = e^b > 1$. As a consequence, when γ approaches zero (i.e., once the mean LLR falls below a certain level), the input to the inverse function $\phi^{-1}(\cdot)$ of (20) fails to approach one and thus γ cannot become zero, rendering further polarization effects untraceable. The second issue is due to the fact that the function $\phi(\gamma)$ takes a value in the interval $(0, 1)$ and can thus approach arbitrarily close to zero as γ becomes large. For example, when $\gamma = 1000$, which is a typical value in the case of polar codes with relatively large code length, we observe that $\phi(\gamma) \approx 1.49 \times 10^{-110}$. Since its inverse function $\phi^{-1}(\cdot)$ cannot be expressed in a closed form, one should resort to numerical approaches such as the bisection method for improving the numerical accuracy. As γ becomes large (i.e., once the mean LLR exceeds a certain level), however, numerically computing the inverse function fails to return an accurate value even with the bisection method, and thus again makes further polarization untraceable¹. These issues can be solved by the proposed log-domain calculation technique of the function $\phi(\gamma)$ described in what follows.

Remark 1: The fact that the approximation suggested by Chung *et al.* should result in $\lim_{\gamma \rightarrow 0} \phi(\gamma) > 1$ was identified by Ha *et al.* [18], in conjunction with designing *punctured* LDPC codes. (This

¹As we shall discuss in Remark 3 of Section III-C, once the mean LLR of given channels exceeds some large value at a given stage, it may diminish slowly even if it experiences \boxplus operations in later stages. Therefore, one may stop further tracing for these channels as they are most likely to be selected as information bits.

fact has been also pointed out in [24] in the framework of polar code design with long codewords.) Therefore, in addition to (21), the following correction has been proposed:

$$\phi(\gamma) \approx e^{\alpha\gamma + \beta\gamma^2}, \quad \text{for } 0 < \gamma < \Gamma'_{\text{th}}, \quad (24)$$

where $\alpha = -0.4856$, $\beta = 0.0564$, and $\Gamma'_{\text{th}} = 0.867861$. This approach resolves the issue associated with the numerical inaccuracy of the original GA as $\gamma \rightarrow 0$. Similar expressions have been developed in [24].

B. Log-Domain Expression for $\phi(\gamma)$

Recall that the mean LLR of polar codes at the code construction design stage should range from very small values to very large values, and the metric calculation associated with GA should support this exponential range. For example, if the design SNR is 1 (i.e., 0 dB), then the initial mean LLR value should be $\gamma_0 = 4$. For a polar code with $N = 2^n$, since each operation of (13) doubles the LLR value as shown in (14), the largest value (after n stages) is $L_{\text{max}} = 4 \times 2^n$. On the other hand, the amount of change from $\gamma_{k-1}^{(i)}$ to $\gamma_k^{(2i)}$ according to (12) depends on its input value, and as is observed from Fig. 1, its ratio $\gamma_k^{(2i)}/\gamma_{k-1}^{(i)}$ rapidly becomes smaller as $\gamma_{k-1}^{(i)}$ decreases and the ratio becomes much less than 1/2 with small enough $\gamma_{k-1}^{(i)}$. Therefore, in order to track the mean values by GA accurately, $\gamma_k^{(2i)}$ must be precisely calculated even if it becomes extremely small as discussed in the previous subsection.

To cope with this issue, we define the logarithmic domain of $\phi(\gamma)$ as

$$\xi(\gamma) \triangleq \log \phi(\gamma) = \log(1 - \psi(\gamma)) \quad (25)$$

and based on this function we attempt to trace the mean LLR value. Note that $\xi(\gamma) : (0, \infty) \rightarrow (-\infty, 0)$, and $\xi(\gamma)$ is monotonically decreasing with γ . Two major advantages of using (25) are that i) as $\gamma \rightarrow 0$, $\xi(\gamma) \approx -\psi(\gamma)$ since $\psi(\gamma) \rightarrow 0$ as well, and thus $\xi(\gamma)$ can accurately trace γ in this regime as well, and ii) for $\gamma \rightarrow \infty$, then $\psi(\gamma) \rightarrow 1$, and it will be shown that $\xi(\gamma)$ is, to first order, linear in γ , and thus γ can again be accurately traced in this regime. By comparison, when γ is large, $\psi(\gamma) \approx 1$ (see Fig. 1), and $\psi(\gamma)$ would need to be computed with very high precision to obtain γ from its inverse as even a slight error in $\psi(\gamma)$ can result in an incorrect inverse γ . Therefore, we first develop the asymptotic forms of $\xi(\gamma)$ for low and high values of γ .

1) *Asymptotic Form of $\xi(\gamma)$ for Small Values of γ* : We first note that the following lemma holds for the function $\psi(\gamma)$:

Lemma 1: For $\psi(\gamma)$ defined in (16), we have

$$\psi(\gamma) = \frac{1}{2}\gamma - \frac{1}{4}\gamma^2 + \frac{5}{24}\gamma^3 + O(\gamma^4) \quad \text{as } \gamma \rightarrow 0. \quad (26)$$

The proof is given in Appendix A.

From Lemma 1, the following theorem is immediate by a Maclaurin series expansion of $\xi(\gamma)$:

Theorem 1: For $\xi(\gamma)$ defined in (25), we have

$$\xi(\gamma) = -\frac{1}{2}\gamma + \frac{1}{8}\gamma^2 - \frac{1}{8}\gamma^3 + O(\gamma^4) \quad \text{as } \gamma \rightarrow 0. \quad (27)$$

2) *Asymptotic Form of $\xi(\gamma)$ for Large Values of γ* : In this case, we may make use of the following expression:

Theorem 2: For $\xi(\gamma)$ defined in (25), we may express

$$\xi(\gamma) = -\frac{\gamma}{4} + \frac{1}{2} \log \pi - \frac{1}{2} \log \gamma + \log \left(1 - \frac{\pi^2}{4\gamma} + O\left(\frac{1}{\gamma^2}\right) \right) \quad \text{as } \gamma \rightarrow \infty. \quad (28)$$

Proof: By applying the identity $\tanh(x/2) = 1 - 2/(e^x + 1)$ to (16), we may rewrite (19) directly through series expansion as

$$\begin{aligned} \phi(\gamma) &= \frac{1}{\sqrt{\pi\gamma}} \int_{-\infty}^{\infty} \frac{1}{e^x + 1} e^{-\frac{(x-\gamma)^2}{4\gamma}} dx \\ &= \frac{e^{-\frac{\gamma}{4}}}{\sqrt{\pi\gamma}} \int_{-\infty}^{\infty} \frac{e^{\frac{x}{2}}}{e^x + 1} e^{-\frac{x^2}{4\gamma}} dx \\ &= \frac{e^{-\frac{\gamma}{4}}}{\sqrt{\pi\gamma}} \int_{-\infty}^{\infty} \frac{e^{\frac{x}{2}}}{e^x + 1} \sum_{k=0}^{\infty} \frac{1}{k!} \left(-\frac{x^2}{4\gamma}\right)^k dx \\ &= \frac{e^{-\frac{\gamma}{4}}}{\sqrt{\pi\gamma}} \sum_{k=0}^{\infty} \frac{(-1)^k}{k!(4\gamma)^k} \int_{-\infty}^{\infty} x^{2k} \frac{e^{\frac{x}{2}}}{e^x + 1} dx \\ &= \frac{e^{-\frac{\gamma}{4}}}{\sqrt{\pi\gamma}} \sum_{k=0}^{\infty} \frac{(-1)^k}{(16\gamma)^k} \frac{(2k)!}{k!} \left\{ \zeta\left(2k+1, \frac{1}{4}\right) - \zeta\left(2k+1, \frac{3}{4}\right) \right\} \\ &= \frac{e^{-\frac{\gamma}{4}}}{\sqrt{\gamma}} \sqrt{\pi} \left(1 - \frac{\pi^2}{4\gamma} + \frac{5\pi^4}{32\gamma^2} - \frac{61\pi^6}{384\gamma^3} + \dots \right), \end{aligned} \quad (29)$$

where $\zeta(m, q)$ is the generalized Riemann zeta function defined as

$$\zeta(m, q) = \sum_{l=0}^{\infty} \frac{1}{(l+q)^m}. \quad (30)$$

Taking logarithm of both sides of (29) leads to (28). ■

Note that the asymptotic case of Theorem 2 agrees with the bounds developed in [6], i.e., (22).

3) *Closed-Form Approximation:* Given the above observations of $\xi(\gamma)$ in term of limiting behavior, the remaining issue is how to describe its closed form approximation $\hat{\xi}(\gamma)$ for each value of γ . We propose the following expression:

$$\hat{\xi}(\gamma) = \begin{cases} -\frac{1}{2}\gamma + \frac{1}{8}\gamma^2 - \frac{1}{8}\gamma^3, & \gamma \leq \Gamma_0, & (31a) \\ a_0 + a_1\gamma + a_2\gamma^2, & \Gamma_0 < \gamma \leq \Gamma_1, & (31b) \\ a\gamma^c + b, & \Gamma_1 < \gamma < \Gamma_2, & (31c) \\ -\frac{\gamma}{4} + \frac{1}{2}\log \pi - \frac{1}{2}\log \gamma + \log \left(1 - \frac{\pi^2}{4\gamma} + \frac{\kappa_0}{\gamma^2}\right), & \Gamma_2 \leq \gamma, & (31d) \end{cases}$$

where the parameters in (31b) are chosen as $(a_0, a_1, a_2) = (-0.002706, -0.476711, 0.0512)$, those in (31c) are adopted as $(a, b, c) = (-0.4527, 0.0218, 0.86)$ following Chung *et al.*, and $\kappa_0 = 8.554$, with the thresholds chosen as $\Gamma_0 = 0.2$, $\Gamma_1 = 0.7$, and $\Gamma_2 = 10$.

Each expression in (31) is chosen as follows: When γ is close to zero, (31a) results from Theorem 1, whereas the expression (31c) is inherited from the work of Chung *et al.* [6], i.e., (21). For a given pair of thresholds Γ_0 and Γ_1 , the intermediate expression (31b) is obtained by curve fitting, where a_2 is optimized through an exhaustive search such that it minimizes the squared error from the function calculated by numerical integration, provided that the piece-wise continuity should be guaranteed at the boundaries Γ_0 and Γ_1 by selection of the parameters a_0 and a_1 . Finally, for large values of γ , (31d) is adopted with reference to (28), where we have introduced a positive constant κ_0 as a fitting parameter that minimizes the squared error in the range $(\Gamma_2, \Gamma_2 + 2)$. It is clear that the impact of κ_0 becomes negligible as γ increases.

Remark 2: Note that the modified approximation formula proposed by Ha *et al.* [18], i.e., (24), has strong similarity with the theoretical limit of (31a) if it is converted to the log domain. Therefore, it may be capable of capturing the polarization effect in the case of $\gamma \rightarrow 0$, similar to the proposed approach based on the log-domain analysis. The corresponding approximate function (31) together with those calculated using the conventional GA of (21) as well as its modification of (24) by Ha *et al.* are compared in Fig. 2. Even though all the approximate curves exhibit good agreement with that based on the numerical calculation, they reveal some difference in the proximity of $\gamma = 0$. The conventional expression (21) exceeds 0, whereas a slight difference is observed with the modification in (24). As expected, the proposed expression yields no discernible difference from the curve calculated by numerical integration for γ near 0.



Fig. 2. Comparison of the function $\xi(\gamma)$ calculated through numerical integration and its piece-wise approximate form $\hat{\xi}(\gamma)$ through (31a)–(31d). Also plotted are the corresponding curves based on the conventional GA by Chung *et al.* [6] and its modified version by Ha *et al.* [18]. The area around the origin is enlarged as a reference.

C. Proposed Log-Domain GA Algorithm

Given the expression of $\xi(\gamma)$, the mean LLR value associated with (20) can be rewritten with respect to $\xi(\gamma)$ as

$$\gamma_k^{(2i)} = \xi^{-1} \left(\xi \left(\gamma_{k-1}^{(i)} \right) + \log \left(2 - e^{\xi \left(\gamma_{k-1}^{(i)} \right)} \right) \right), \quad (32)$$

whereas $\gamma_k^{(2i+1)}$ is revised according to (14).

The inverse function of $z = \hat{\xi}(\gamma)$, i.e., $\hat{\xi}^{-1}(z) : (-\infty, 0) \rightarrow (0, \infty)$ can be obtained by solving the corresponding equations as

$$\hat{\xi}^{-1}(z) = \begin{cases} -2z + z^2 + z^3, & z \geq Z_0, & (33a) \\ \frac{-a_1 - \sqrt{a_1^2 - 4a_2(a_0 - z)}}{2a_2}, & Z_1 \leq z < Z_0, & (33b) \\ \left(\frac{z - b}{a} \right)^{\frac{1}{c}}, & Z_2 < z < Z_1, & (33c) \end{cases}$$

where the Z_i 's are the thresholds of the two functions, i.e., $Z_i = \hat{\xi}(\Gamma_i)$. Note that (33a) is obtained as an approximation, through series expansion, of the inverse function corresponding to (31a). In the case of $z \leq Z_2$, the inverse function corresponding to (31d) may not be expressed in closed form. However, it can be easily calculated with high accuracy by using the bisection method.

Algorithm 1 Channel Polarization with Improved GA

Input: $n = \log_2 N$, $\alpha = \text{SNR}_{\text{des}}$
Output: $\gamma[0], \gamma[1], \dots, \gamma[N-1]$ as $\gamma_n^{(0)}, \gamma_n^{(1)}, \dots, \gamma_n^{(N-1)}$

```

1:  $\gamma[0] = 4\alpha$ 
2: for  $i = 1 : n$  do
3:    $J = 2^i$ 
4:   for  $j = 0 : J/2 - 1$  do
5:      $u = \gamma[j]$ 
6:     if  $u \leq \Gamma_0$  then
7:       Update  $\gamma[j]$  with  $u$  as input using (34)
8:     else
9:        $z = \xi(u)$  using (31)
10:       $\gamma[j] = \xi^{-1}(z + \log(2 - e^z))$  using (33)
11:    end if
12:     $\gamma[j + J/2] = 2u$ 
13:  end for
14: end for
15: return  $\gamma[0], \gamma[1], \dots, \gamma[N-1]$ 

```

Furthermore, in the case of $\gamma \leq \Gamma_0$, by substituting $\hat{\xi}(\gamma)$ of (31a) into $\xi(\gamma_{k-1}^{(i)})$ of (32), and then substituting $\hat{\xi}(\gamma) + \log(2 - e^{\hat{\xi}(\gamma)})$ into z of (33a) with series expansion and collecting the dominant terms up to the fourth degree, one may obtain the following expression for $\Xi(\gamma)$ in (17):

$$\Xi(\gamma) \approx \frac{1}{2}\gamma^2 - \frac{1}{2}\gamma^3 + \frac{2}{3}\gamma^4, \quad \gamma \leq \Gamma_0. \quad (34)$$

The improved GA algorithm outlined above is summarized in Algorithm 1.

Remark 3: It would be of interest to investigate how $\Xi(\gamma)$ may behave as $\gamma \rightarrow \infty$. Noticing that the logarithmic term grows substantially slower than the linear term, one may ignore the contribution of the third and fourth terms in (31d) and define the corresponding inverse as $\hat{\xi}^{-1}(z) = -4z + 2\log \pi$. Then, by the same process that has lead to (34), we obtain

$$\Xi(\gamma) \approx \gamma - 4\log 2, \quad \gamma \rightarrow \infty. \quad (35)$$

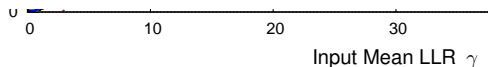


Fig. 3. Comparison of the function $\Xi(\gamma)$ based on Algorithm 1 as well as the other approaches, i.e., the original formula by Chung *et al.* [6], its modification by Ha *et al.* [18], and a piece-wise quadratic function approximation by Trifonov [23], together with the asymptotic form (35). Also shown as “Exact Mean” is the curve representing the theoretical output mean LLR value corresponding to \boxplus operation with Gaussian input $\mathcal{N}(\gamma, 2\gamma)$ based on (41). The two edge areas are enlarged as a reference.

The above approximation indicates that, when the input mean LLR value γ is large, the \boxplus calculation of two independent and equivalent channels, i.e., (8), will reduce the output mean LLR value approximately by $4 \log 2 \approx 2.7726$, whereas it always doubles γ when (9) is applied. In other words, once γ reaches a large enough value where the approximation (35) holds, then the rate at which γ diminishes due to $\Xi(\gamma)$ is much less significant and thus these channels could be selected as information bits even without further high-accuracy tracing.

Remark 4: Fig. 3 shows the relationship between the input and output mean LLR values, i.e., the function $\Xi(\gamma)$, obtained through the improved GA as well as those calculated by the other schemes discussed above. Also plotted are the linear asymptote given by (35) and the mean LLR value directly calculated without assuming the GA model for later reference (to be discussed in Remark 5 at the end of this section). We observe some noticeable discrepancy between the improved GA and the original GA as γ approaches zero. However, the improved approximation by Ha *et al.* resembles that of the improved GA developed here. Also observed is the fact that the simple approximation (35) becomes tighter as γ increases. We note that instead of dealing with the function $\phi(\gamma)$ and its inverse, Trifonov [23] introduces a direct approximation of $\Xi(\gamma)$ by a piece-wise quadratic function, which is also plotted in Fig. 3 for comparison. This approach may significantly simplify the design of polar codes and it turns out to be effective for constructing

a wide range of polar codes with moderate lengths. However, we observe that there is some discrepancy especially in the low value of γ as our analysis suggests that their asymptotic form should follow (34), i.e., the quadratic approximation may have some non-negligible numerical gap. This will affect the achievable performance of the code designed for long code lengths and low code rate as will be demonstrated in Section V.

D. Block Error Rate Estimation

As discussed in [2], [4], [8], once the distribution of LLRs is determined by density evolution or the GA method, its block error rate (BLER) based on SC decoding can also be estimated. Assuming that the all zero codeword is transmitted, the bit error probability of the i th bit, provided that all the previous bits are correctly decoded, is given by

$$P_{b,i} = \Pr(\hat{u}_i \neq 0 | \hat{u}_0 = \dots = \hat{u}_{i-1} = 0) = \Pr(L_n^{(i)} < 0), \quad (36)$$

and under the assumption that $L_n^{(i)} \sim \mathcal{N}(\gamma_n^{(i)}, 2\gamma_n^{(i)})$, it follows that

$$P_{b,i} = Q\left(\sqrt{\frac{\gamma_n^{(i)}}{2}}\right), \quad (37)$$

where the Q -function $Q(x) : [0, \infty) \rightarrow (0, \frac{1}{2}]$ is defined as $Q(x) = \frac{1}{2}\text{erfc}\left(\frac{x}{\sqrt{2}}\right) = \frac{1}{\sqrt{2\pi}} \int_x^\infty e^{-\frac{t^2}{2}} dt$.

The BLER is often approximated as

$$P_{BL} \approx 1 - \prod_{i=0}^{N-1} (1 - P_{b,i}). \quad (38)$$

In the process of polar code design, let $\hat{\gamma}_n^{(i)}(\alpha)$, $i \in \{0, 1, \dots, N-1\}$, denote the estimated output mean LLR obtained by some GA algorithm with α as its initial input SNR. If we select the set of K channel indices with largest outputs as the information set \mathcal{I} , the minimum BLER with a given rate $R = K/N$ can be achieved. We define the resulting *minimum estimated BLER* for a given design SNR as

$$\hat{P}_{BL,\min}(R, \text{SNR}_{\text{des}}) \triangleq \min_{\mathcal{I}: |\mathcal{I}|=RN} \left\{ 1 - \prod_{i \in \mathcal{I}} \left(1 - Q\left(\sqrt{\frac{\hat{\gamma}_n^{(i)}(\text{SNR}_{\text{des}})}{2}}\right) \right) \right\}. \quad (39)$$

For a given pair of design SNR and code rate, the above BLER can be calculated by sorting $\hat{\gamma}_n^{(i)}(\text{SNR}_{\text{des}})$ in decreasing order (after applying a specific GA algorithm) and selecting only the largest $|\mathcal{I}|$ elements from the entire index set $\{0, 1, \dots, N-1\}$. Note that the above estimated performance corresponds to the scenario where a code is designed for a specific SNR value and

therefore this performance is achieved by a *family* of polar codes with SC decoding, possibly employing a different information set at each SNR.

The above relationship can also be utilized for evaluating the estimated performance of a *given designed polar code*. Let \mathcal{I}^* denote the information set designed through the above process, i.e., the set \mathcal{I} that yields the minimum estimated BLER evaluated at a given design SNR well below a target BLER according to (39). The resulting estimated BLER of the specific polar code defined by \mathcal{I}^* , evaluated at a given *channel SNR*, may be defined as

$$\hat{P}_{BL}(\mathcal{I}^*, E_s/N_0) \triangleq 1 - \prod_{i \in \mathcal{I}^*} \left(1 - Q \left(\sqrt{\frac{\hat{\gamma}_n^{(i)}(E_s/N_0)}{2}} \right) \right). \quad (40)$$

It is easy to see that (39) serves as a lower bound on (40). Moreover, if \mathcal{I}^* of (40) is designed with SNR_{des} through (39), then both BLER values should agree at the channel SNR where the equality $E_s/N_0 = \text{SNR}_{\text{des}}$ holds.

Remark 5: We end this section by pointing out an intriguing fact of GA. Even though the initial LLR of bit channels $L_0^{(0)}$ is Gaussian distributed, there is no guarantee that $L_k^{(2i)}$ is Gaussian since the output after \boxplus operation, i.e., (8), is not strictly Gaussian. However, the notable aspect associated with the use of (15) is that even if $L_k^{(2i)}$ is not Gaussian, the mean $\gamma_k^{(2i)}$ is chosen such that $L_k^{(2i)}$ is *approximated* by a Gaussian with mean $\gamma_k^{(2i)}$ and variance $2\gamma_k^{(2i)}$. Therefore, the computed $\gamma_k^{(2i)}$ will be different from a direct calculation of the LLR mean:

$$E \left[L_k^{(2i)} \right] = 2E \left[\tanh^{-1} \left\{ \tanh \left(\frac{L_{k-1}^{(i)}}{2} \right) \tanh \left(\frac{L_{k-1}^{(i)'}}{2} \right) \right\} \right]. \quad (41)$$

In APPENDIX B, the above mean value is theoretically derived, and the results are compared in Fig. 3 with the mean LLR obtained by the (improved) GA for a given input mean LLR. From the figure, we observe that the behavior of the two functions are significantly different, especially as the mean input LLR increases. Due to this difference, the polar code design using the mean LLR directly calculated through (41) may not lead to the same result as the GA approach through (15), and their performance is in general inferior to those designed by GA.

IV. AN ALTERNATIVE CONSTRUCTION BASED ON LLR FLIPPING PROBABILITY

In the previous section, we discussed numerical issues associated with mean LLR calculation in the GA method, and how to cope with them. However, the non-linearity of \tanh does not strictly preserve the Gaussianity of the distribution of the LLR. In this section, we consider

an alternative approach that avoids the use of the \boxplus operation upon calculation of the metric associated with check nodes by only tracking the probability where the LLR value is reversed. We refer to this construction approach as the *LLR flipping probability construction*. The resulting equations can be implemented with much less elaboration than GA, but it still requires the assumption that the LLR is Gaussian distributed. Numerical results will also reveal that such an approach is still effective for constructing polar codes with moderate length. We recognize that the same approach described here was independently proposed by Tahir and Rupp in [25]. For the purpose of comparison, we briefly describe this simple and tractable approach based on our own understanding.

From the relationship of the check node given in (8), it is easy to observe that

$$\text{Event} \left[L_k^{(2i)} < 0 \right] = \text{Event} \left[\left(L_{k-1}^{(i)} < 0 \cap L_{k-1}^{(i)'} > 0 \right) \cup \left(L_{k-1}^{(i)} > 0 \cap L_{k-1}^{(i)'} < 0 \right) \right]. \quad (42)$$

Since the two events under the union operation in the right hand side of (42) are mutually exclusive, we may express

$$\begin{aligned} \Pr \left(L_k^{(2i)} < 0 \right) &= \Pr \left(L_{k-1}^{(i)} < 0 \cap L_{k-1}^{(i)'} > 0 \right) + \Pr \left(L_{k-1}^{(i)} > 0 \cap L_{k-1}^{(i)'} < 0 \right) \\ &= \Pr \left(L_{k-1}^{(i)} < 0 \right) \Pr \left(L_{k-1}^{(i)'} > 0 \right) + \Pr \left(L_{k-1}^{(i)} > 0 \right) \Pr \left(L_{k-1}^{(i)'} < 0 \right) \\ &= 2 \Pr \left(L_{k-1}^{(i)} < 0 \right) \left[1 - \Pr \left(L_{k-1}^{(i)} < 0 \right) \right] \end{aligned} \quad (43)$$

where the last two equalities stem from the fact that $L_{k-1}^{(i)}$ and $L_{k-1}^{(i)'}$ are i.i.d. The above equation shows that the flipping probability of the LLR output from the check node is given by that of the input LLR. Therefore, the evolution of LLR through the check node can be traced through (43) if its flipping probability is of interest. However, the LLR evaluation through the variable node, i.e., calculation of (9) cannot be performed through this approach unless we know the distribution of the input LLR. Therefore, analogous to GA we assume that input LLR is Gaussian distributed with mean μ and variance σ^2 , i.e., $L_{k-1}^{(i)} \sim \mathcal{N}(\mu, \sigma^2)$. Then, it follows that $L_k^{(2i+1)} \sim \mathcal{N}(2\mu, 2\sigma^2)$ and therefore

$$\Pr \left(L_{k-1}^{(i)} < 0 \right) = Q \left(\sqrt{\frac{\mu^2}{\sigma^2}} \right), \quad (44)$$

$$\Pr \left(L_k^{(2i+1)} < 0 \right) = Q \left(\sqrt{\frac{2\mu^2}{\sigma^2}} \right). \quad (45)$$

Consequently, we may write

$$\Pr \left(L_k^{(2i+1)} < 0 \right) = Q \left[\sqrt{2} Q^{-1} \left(\Pr \left(L_{k-1}^{(i)} < 0 \right) \right) \right], \quad (46)$$

Algorithm 2 Channel Polarization with LLR Flipping Probability

Input: $n = \log_2 N$, $\alpha = \text{SNR}_{\text{des}}$
Output: $p[0], p[1], \dots, p[N-1]$ as $\Pr(L_n^{(0)} < 0)$, $\Pr(L_n^{(1)} < 0)$, \dots , $\Pr(L_n^{(N-1)} < 0)$

```

1:  $p[0] = Q(\sqrt{2\alpha})$ 
2: for  $i = 1 : \log_2 N$  do
3:    $J = 2^i$ 
4:   for  $j = 0 : J/2 - 1$  do
5:      $z = p[j]$ 
6:      $p[j] = 2z(1 - z)$ 
7:      $p[j + J/2] = Q[\sqrt{2}Q^{-1}(z)]$ 
8:   end for
9: end for
10: return  $p[0], p[1], \dots, p[N-1]$ 

```

where $Q^{-1}(\cdot) : (0, \frac{1}{2}] \rightarrow [0, \infty)$ is the *inverse Q-function* with $Q^{-1}[Q(x)] = x$, which can be calculated numerically through the bisection method.

Note that since $L_0^{(0)} \sim \mathcal{N}(\gamma_0, 2\gamma_0)$, we have

$$\Pr(L_0^{(0)} < 0) = Q\left(\sqrt{\frac{\gamma_0}{2}}\right) = Q\left(\sqrt{\frac{2E_s}{N_0}}\right), \quad (47)$$

which is simply the bit error rate (BER) of uncoded BPSK as expected.

The channel polarization probability computation based on LLR flipping is summarized in Algorithm 2. Let \hat{p}_i denote the resulting estimated flipping probability $\Pr(L_n^{(i)} < 0)$ obtained by the algorithm with SNR_{des} as its design SNR. Then, similar to (39) in the case of GA, the minimum estimated BLER can be defined as

$$\hat{P}_{BL,\min}(R, \text{SNR}_{\text{des}}) \triangleq \min_{\mathcal{I}: |\mathcal{I}|=RN} \left\{ 1 - \prod_{i \in \mathcal{I}} (1 - \hat{p}_i) \right\} \quad (48)$$

and thus selecting the channel indices with the smallest flipping probabilities $\Pr(L_n^{(i)} < 0)$ may lead to the minimization of the resulting BLER. Likewise, the estimated performance of a given designed polar code can be expressed in a similar form to (40).

Since the function $Q(\cdot)$ returns a probability, it can rapidly approach 1/2 or 0 through the transformation of (43). To improve numerical stability, one may use a log-domain approach

similar to the improved GA described in this paper. For simplicity, this issue will not be discussed further. The design based on the LLR flipping probability depends on how accurate the Gaussian modeling associated with (46) is. It should be mentioned that the output LLR after \boxplus operation is not Gaussian in general. Therefore, calculating the equivalent mean LLR value through the inverse Q-function shown in (46) may not be necessarily accurate and error may accumulate as this process is repeated. If this part can be implemented with a more accurate model, the performance (both BLER estimation and actual simulation based on this construction) would be further improved.

V. CODE DESIGN AND PERFORMANCE EXAMPLES

In this section, we investigate the performance of polar codes designed by the code constructions described in the previous sections through Monte-Carlo simulations as well as the corresponding BLER estimates. Throughout all simulations, we employ the exact LLR calculations².

A. Effect of Design SNR

As an initial process of polar code design based on GA, we investigate the effect of a design SNR value on the resulting BLER performance. To this end, we first evaluate the minimum estimated BLER, achieved by a *family* of polar codes, as a function of the design SNR based on (39). We then evaluate the estimated BLER of *specific* polar codes constructed at a given design SNR, as a function of channel SNR based on (40), and compare with the corresponding simulation results. In these steps, we employ Algorithm 1, where the inverse function corresponding to (31d) is calculated by the bisection method. The results are shown in Fig. 4 for the polar codes with code length $n = 16$ ($N = 65\,536$) and code rate $R = 1/2$. For the purpose of demonstration, we have selected three different design SNR values as follows: We first fix the *target* design SNR as $\text{SNR}_{\text{des}} = -1.48$ dB, by observing where the minimum estimated BLER curve (39) achieves the target BLER (set between 10^{-4} and 10^{-3}). The two other design SNR values are chosen to be either higher (+0.65 dB) or lower (-0.65 dB) than this target value. The comparison of the three curves clearly reveals that if the design SNR is set

²Specifically, all the terms of (54) in APPENDIX B are used for LLR calculation. This is in contrast to the suboptimal min-sum decoder that calculates only the first term of (54).

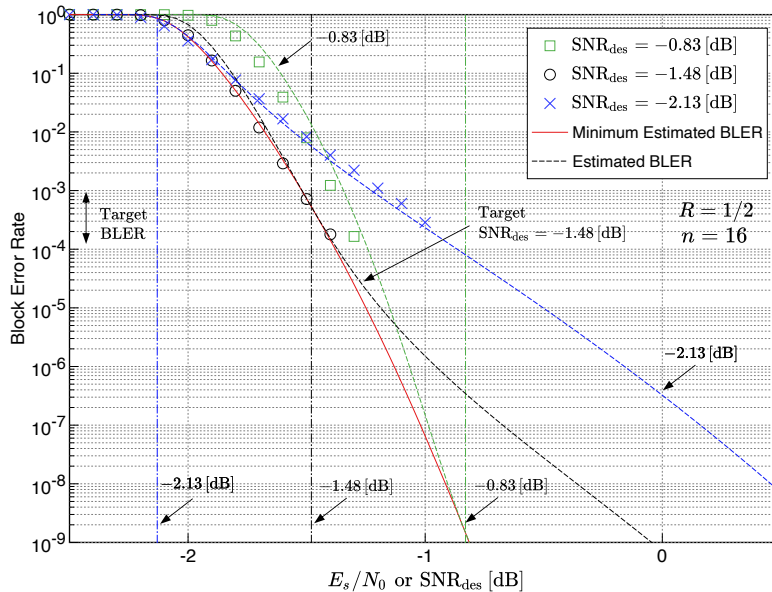


Fig. 4. Comparison of minimum estimated BLER for a family of polar codes, estimated BLER for the polar codes designed at specific design SNR, and the corresponding simulation results, all designed using Algorithm 1. The code length is $n = 16$ ($N = 65\,536$) and code rate is $R = 1/2$.

too low, the generated polar code performs better only in the low SNR region (of less practical interest), and *vice versa*. We also notice that the polar code designed with an SNR targeting a BLER of 10^{-3} could perform worse than that designed at higher SNR targeting a lower BLER when they are compared by the required E_s/N_0 in order to achieve a BLER below 10^{-5} . This clearly demonstrates the importance of the design SNR parameter selection based on the target BLER, and the minimum estimated BLER curves serve as a good initial starting point. For the rest of the numerical results, we will select the design SNR such that the resulting minimum estimated BLER should fall between 10^{-4} and 10^{-3} .

Remark 6: It may be worthwhile to point out the complexity required for calculating these estimated curves. Upon evaluating the minimum estimated BLER of (39), Algorithm 1 should be performed for each value of the design SNR, which has complexity of $O(N)$. After obtaining the estimated SNR $\hat{\gamma}_n^{(i)}$ for all N channels, the highest K values should be selected for the information set \mathcal{I} (or the lowest $N - K$ values for the frozen set \mathcal{I}^c). The complexity of this process is $O(N \log N)$, which becomes non-negligible as N increases. However, the estimated SNR values of most channels are either close to 0 (bad channels) or approaching ∞ (good channels) due to polarization. Therefore, one can eliminate these good and bad channels prior to sorting, since they are always selected as information and frozen bits, respectively. With this pre-

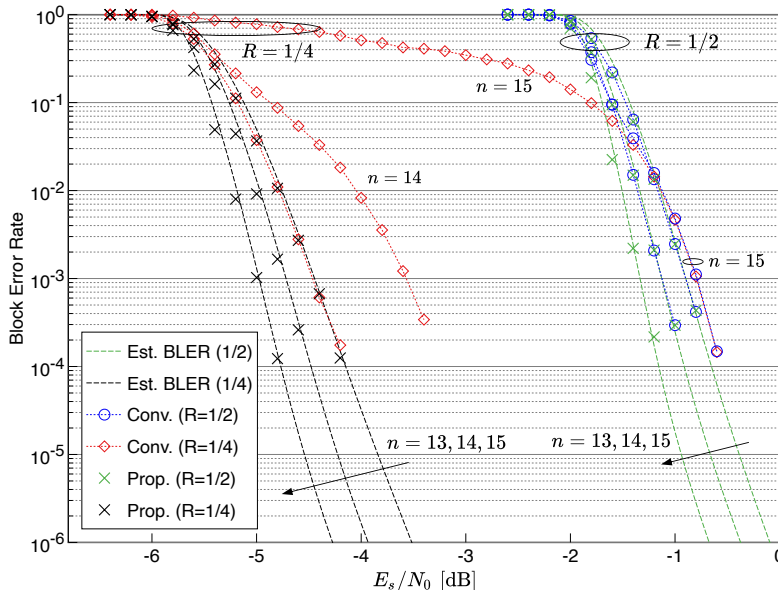


Fig. 5. Comparison of simulated BLER for the conventional and improved GA with code rate $R = 1/2$ and $1/4$. The code length is given by $N = 2^n$, with $n = 13, 14$, and 15 ($N = 8192, 16384$, and 32768). The corresponding estimated BLER curves as a function of E_s/N_0 based on the improved GA are also plotted as a reference.

processing, the required time to calculate (39) becomes negligible even for very long codeword cases. Once the optimal information set \mathcal{I}^* is obtained for a given design SNR, the evaluation of the estimated BLER (40) can be performed by running Algorithm 1 again with each given channel SNR as its input, and the resulting complexity is also negligible.

B. Comparison with Conventional GA and Improved GA

We now compare the BLER performance of the conventional and improved GA through Monte-Carlo simulations and demonstrate how the BLER of conventional GA diverges from the estimated BLER as the code length increases. Fig. 5 shows the simulation results of polar codes constructed at the design SNR as described in the previous subsection. The corresponding estimated BLER curves with respect to E_s/N_0 based on the improved GA are also plotted as a reference. For the conventional GA, we apply (21) and (23), where the bisection method is used for calculating the inverse function of (23). The two code rate cases of $R = 1/2$ and $1/4$ are evaluated with the code length ranging from $N = 2^{13} = 8192$ to $N = 2^{15} = 32768$. We observe that the polar codes constructed by the two GA perform almost identical up to some code length as expected, but start to diverge beyond $n = 14$ for $R = 1/4$, whereas the performance of the improved GA follows similar to the estimated BLER regardless of code length. It is

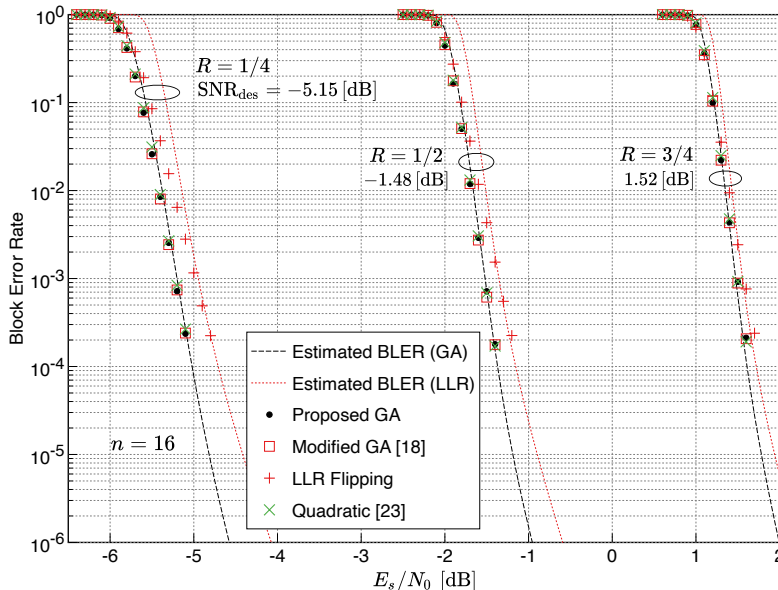


Fig. 6. Comparison of BLER for the polar codes constructed by Algorithm 1 (improved GA), Algorithm 2 (LLR flipping), the modified GA by Ha *et al.* [18], and a quadratic function approximation by Trifonov [23]. The corresponding estimated BLER curves derived from Algorithms 1 and 2 are also plotted.

also interesting to note that for the conventional GA with $n = 15$, the two BLER curves *with different code rate* eventually merge, which suggests that they share the same weak channels in the information set due to numerical inaccuracy of the conventional GA, and this inaccuracy dominates the performance of SC decoding.

C. Comparison among GA-Based Approaches and LLR Flipping Probability with $n = 16$

Next, we compare the performances of polar codes constructed by the GA-based approaches and the LLR flipping probability. As an example of relatively large code length, we select $n = 16$ ($N = 65\,536$). For construction based on the GA, we have simulated three specific cases, i.e., the modified GA by Ha *et al.* [18], the quadratic approach by Trifonov [23], and the proposed GA based on Algorithm 1. Note that since the quadratic approach [23] does not require any calculation associated with the inverse function of $\phi(\gamma)$ or $\xi(\gamma)$, it requires the shortest time to generate an information set among all the others compared here. All the polar codes compared are generated with the same design SNR for a given code rate³.

³The best design SNR that yields the minimum required E_s/N_0 in order to achieve a given target BLER should be different for each scheme. However, in all the simulation results, we construct each code with the identical design SNR value for the purpose of demonstration.

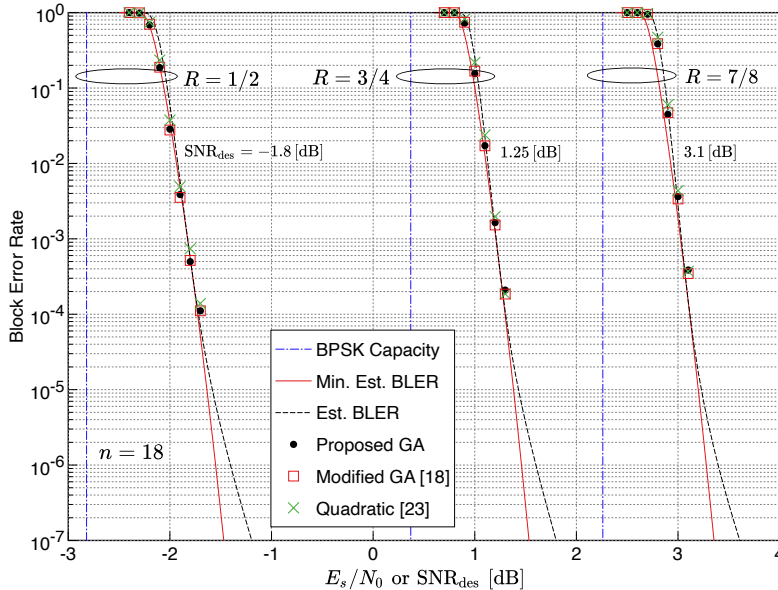


Fig. 7. BLER comparison of long polar codes (with $n = 18$) based on the three GA-based construction schemes with code rate above $1/2$. The minimum estimated BLER curves as a function of design SNR, as well as the estimated BLER for each polar code simulated here, are also plotted using Algorithm 1.

The results are shown in Fig. 6 with code rates $R = 1/4$, $1/2$, and $3/4$, where the estimated BLER calculated by the improved GA method and that by the LLR flipping probability method are also plotted as a reference. We observe that there is some difference in terms of the estimated BLER between the improved GA and LLR flipping probability methods, and the gap becomes larger as the code rate decreases. The corresponding simulation results also indicate that the code designed by the LLR flipping probability method is worse than those constructed by the modification of GA method. Therefore, even though both approaches are based on the assumption of Gaussian distribution for LLR, the GA-based approach may be more effective in terms of polar code design. Furthermore, the polar codes designed by the three GA approaches exhibit similar performance. Therefore, the difference among them is not clear from this codeword length even with various code rates.

D. Comparison of GA Schemes with $n = 18$

Finally, we focus on even longer polar codes and evaluate the performance difference among the three GA-based approaches. The code length is set as $N = 262144$ ($n = 18$) and the code rates R are selected from $1/8$ (0.125) up to $7/8$ (0.875). In Fig. 7, the BLERs for the cases with higher code rates are compared, whereas Fig. 8 compares the BLER for the lower code

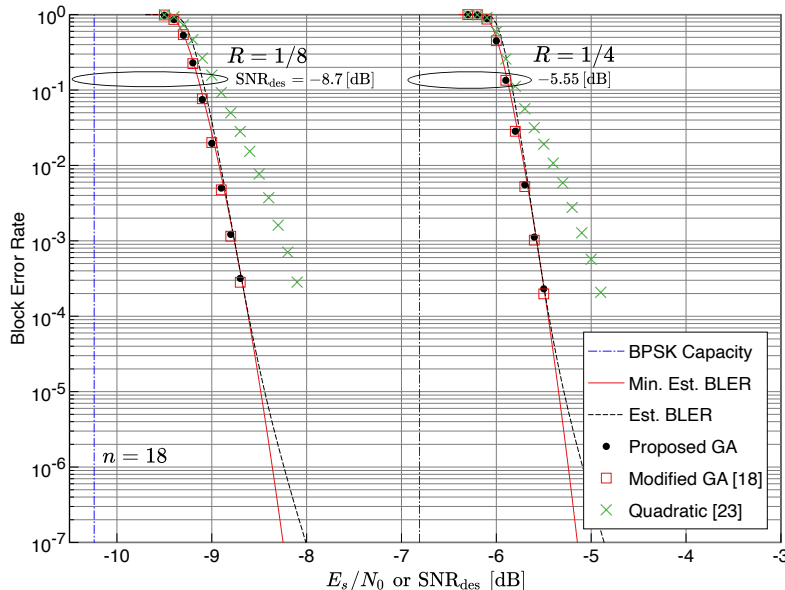


Fig. 8. BLER comparison of long polar codes (with $n = 18$) based on the three GA-based construction schemes with very low code rate. The minimum estimated BLER curves as a function of design SNR, as well as the estimated BLER for each polar code simulated here, are also plotted using Algorithm 1.

rate cases. In all the results, the minimum estimated BLER curves as a function of design SNR with a fixed code rate, as well as the estimated BLER curves as a function of channel SNR, both employing Algorithm 1, are plotted. Also shown are the corresponding theoretical limits (the minimum E_s/N_0 values required to achieve the corresponding information rates in terms of the BPSK channel capacity).

From the results, we observe that the simulation results of the polar codes constructed based on the proposed GA with a given design SNR agree well with the estimated BLER evaluated at the same design SNR, especially in the BLER range of practical interest ($10^{-2} - 10^{-3}$). Comparing the three GA approaches, the polar codes based on the quadratic formula show some degradation from the other two constructions as the channel E_s/N_0 becomes lower (i.e., lower code rate cases). This may stem from the fact that the quadratic approximation of the function $\Xi(\gamma)$ shows some discrepancy from the more precise approaches as observed in Fig. 3. On the other hand, the proposed GA and the modified GA by Ha. *et al.* show similar BLER performances⁴, which can also be confirmed from Fig. 3 as they have close resemblance even

⁴Numerical comparison has indicated that for the polar codes of $n = 18$ constructed by the two GA schemes compared here, approximately 99.7% of the frozen bits agrees when $R = 3/4$ and $7/8$, 99.9% when $R = 1/2$, and 99.96% when $R = 1/4$ and $1/8$.

in the very low range of γ .

VI. CONCLUSIONS

We have discussed a construction of polar codes with large code lengths based on an improved GA as well as LLR flipping probability assuming simple SC decoding. For the former, we have developed closed-form expressions that allow us to precisely calculate the nonlinear function associated with GA for asymptotic cases of low and high SNR based on its series expansion. How to select the design SNR is a key issue for polar code design, and the polar codes designed using the estimated BLER successfully yield capacity approaching behavior as the code length increases. Numerical results have elucidated that the GA-based design approach outperforms that based on the LLR flipping probability.

As a final remark, even if the nonlinear transformation processes such as $\xi(\gamma)$ and $\xi^{-1}(\gamma)$ could be perfectly reproduced by further extending our approach, the optimality of the designed code itself is not at all guaranteed as it is based on an approximation. Therefore, the performance gap from an optimal polar code (that would be identified by more complex design algorithms such as the approach developed by Tal-Vardy) would be of significant interest. Furthermore, the applicability of the expressions based on the log-domain analysis to the design of punctured and shortened polar codes would be worth investigating. We leave these questions for future work.

APPENDIX A

PROOF OF LEMMA 1

Proof: Equation (16) can be expressed as

$$\psi(\gamma) = E \left\{ \tanh \left(\frac{\sqrt{\gamma}}{2} t \right) \right\}, \quad (49)$$

where the expectation is performed over $t \sim \mathcal{N}(\sqrt{\gamma}, 2)$. By the series expansion of the function $\tanh(\cdot)$, we obtain [26]

$$\begin{aligned} \psi(\gamma) &= \sum_{k=1}^{\infty} a_k E \left\{ \left(\frac{\sqrt{\gamma}}{2} t \right)^{2k-1} \right\} \\ &= \sum_{k=1}^{\infty} a_k \left(\frac{\sqrt{\gamma}}{2} \right)^{2k-1} E \{ t^{2k-1} \}, \end{aligned} \quad (50)$$

with the coefficient a_k expressed as

$$a_k = \frac{2^{2k}(2^k - 1)}{(2k)!} B_{2k}, \quad (51)$$

where B_n represents the Bernolli number with its first few even number cases given by $B_2 = \frac{1}{6}$, $B_4 = -\frac{1}{30}$, and $B_6 = \frac{1}{42}$.

The odd-order moment in (50) can be expressed as (see [27] for example)

$$E \{t^{2k-1}\} = \frac{\sqrt{\gamma} (2k)!}{2 k!} {}_1F_1 \left(1 - k; \frac{3}{2}; -\frac{\gamma}{4} \right), \quad (52)$$

where ${}_1F_1(a; b; x)$ is Kummer's confluent hypergeometric function. Substituting (51) and (52) into (50) and after some manipulation, we obtain

$$\psi(\gamma) = \sum_{k=1}^{\infty} \frac{(2^{2k} - 1) B_{2k}}{k!} \gamma^k {}_1F_1 \left(1 - k; \frac{3}{2}; -\frac{\gamma}{4} \right). \quad (53)$$

Note that the function ${}_1F_1(a; b; x)$ is differentiable with respect to x and converges for any finite x . Since ${}_1F_1(0; b; x) = 1$, ${}_1F_1(-1; b; x) = 1 - \frac{x}{b}$, and ${}_1F_1(-2; b; x) = 1 - \frac{2x}{b} + \frac{x^2}{b(1+b)}$, by expanding the terms of (53) up to $k = 3$, we obtain (26). \blacksquare

APPENDIX B

MEAN OF LLR OUTPUT

In this appendix, we derive the mean value of the LLR output associated with the operation $L_o = L_a \boxplus L_b$, assuming that the two input LLRs L_a and L_b are independent Gaussian with $\mathcal{N}(\gamma, 2\gamma)$.

We first note that the output L_o associated with the \boxplus operation of two LLRs L_a and L_b can be expressed by the so-called min-sum form:

$$\begin{aligned} L_o &\triangleq L_a \boxplus L_b \\ &= \underbrace{\text{sign}(L_a) \text{sign}(L_b) \min(|L_a|, |L_b|)}_{\triangleq X} + \log(1 + e^{-|L_a+L_b|}) - \log(1 + e^{-|L_a-L_b|}), \end{aligned} \quad (54)$$

where X corresponds to the output of the min-sum decoder, and is often used as a low-complexity alternative to exact decoding. As discussed in [5], based on the fundamental results on order statistics, the probability density function (pdf) of the random variable X defined above can be expressed as

$$f_X(x) = 2f_L(x) \{1 - F_L(|x|)\} + 2f_L(-x)F_L(-|x|), \quad (55)$$

where $f_L(x)$ and $F_L(x)$ are the pdf and cumulative distribution function (cdf) of L_a (or equivalently L_b), respectively. Assuming $L_a, L_b \sim \mathcal{N}(\gamma, 2\gamma)$, the above pdf can be expressed as

$$f_X(x) = \frac{1}{\sqrt{\pi\gamma}} \left\{ e^{-\frac{(x-\gamma)^2}{4\gamma}} Q\left(\frac{|x|-\gamma}{\sqrt{2\gamma}}\right) + e^{-\frac{(x+\gamma)^2}{4\gamma}} Q\left(\frac{|x|+\gamma}{\sqrt{2\gamma}}\right) \right\}. \quad (56)$$

Next, let us define the random variables $Y = |L_a + L_b|$ and $Z = |L_a - L_b|$ which appear in (54). Since $L_a + L_b \sim \mathcal{N}(2\gamma, 4\gamma)$ and $L_a - L_b \sim \mathcal{N}(0, 4\gamma)$, Y follows a *generalized Rice* distribution and Z follows a *generalized Rayleigh* distribution [28], whose pdfs are expressed as

$$f_Y(y) = \frac{1}{\sqrt{2\pi\gamma}} e^{-\frac{y^2+4\gamma^2}{8\gamma}} \cosh\left(\frac{y}{2}\right) \quad (57)$$

$$f_Z(z) = \frac{1}{\sqrt{2\pi\gamma}} e^{-\frac{z^2}{8\gamma}}. \quad (58)$$

Consequently, the mean of L_o can be expressed as

$$\begin{aligned} E[L_o] &= E[X] + E[\log(1 + e^{-Y})] - E[\log(1 + e^{-Z})] \\ &= \frac{1}{\sqrt{\pi\gamma}} \int_0^\infty \left[z e^{-\frac{(z-\gamma)^2}{4\gamma}} (1 - e^{-z}) \left[Q\left(\frac{z-\gamma}{\sqrt{2\gamma}}\right) - Q\left(\frac{z+\gamma}{\sqrt{2\gamma}}\right) \right] \right. \\ &\quad \left. - \frac{1}{\sqrt{2}} \log(1 + e^{-z}) \left\{ e^{-\frac{z^2}{8\gamma}} - \frac{1}{2} e^{-\frac{1}{8\gamma}(z-2\gamma)^2} (1 + e^{-z}) \right\} \right] dz \quad (59) \end{aligned}$$

$$\begin{aligned} &= \frac{1}{\sqrt{\pi}} \int_0^\infty \left[\sqrt{\gamma} x e^{-\frac{(x-\sqrt{\gamma})^2}{4}} (1 - e^{-\sqrt{\gamma}x}) \left[Q\left(\frac{x-\sqrt{\gamma}}{\sqrt{2}}\right) - Q\left(\frac{x+\sqrt{\gamma}}{\sqrt{2}}\right) \right] \right. \\ &\quad \left. - \frac{1}{\sqrt{2}} \log(1 + e^{-\sqrt{\gamma}x}) \left\{ e^{-\frac{x^2}{8}} - \frac{1}{2} e^{-\frac{1}{8}(x-2\sqrt{\gamma})^2} (1 + e^{-\sqrt{\gamma}x}) \right\} \right] dx, \quad (60) \end{aligned}$$

where (60) may be convenient for small values of γ and (59) is suitable as γ increases for numerical evaluation.

ACKNOWLEDGMENT

The authors would like to thank the editor and reviewers for their constructive comments as well as bringing [18], [23] to the authors' attention.

REFERENCES

- [1] E. Arkan, "Channel polarization: A method for constructing capacity-achieving codes for symmetric binary-input memoryless channels," *IEEE Trans. Inform. Theory*, vol. 55, pp. 3051–3073, 2009.
- [2] R. Mori and T. Tanaka, "Performance of polar codes with the construction using density evolution," *IEEE Commun. Lett.*, vol. 13, pp. 519–521, July 2009.
- [3] T. Richardson, M. A. Shokrollahi, and R. Urbanke, "Design of capacity-approaching irregular low-density parity-check codes," *IEEE Trans. Inform. Theory*, vol. 47, pp. 619–637, Feb. 2001.
- [4] I. Tal and A. Vardy, "How to construct polar codes," *IEEE Trans. Inform. Theory*, vol. 59, pp. 6562–6582, Oct. 2013.
- [5] D. Kern, S. Vorkoper, and V. Kühn, "A new code construction for polar codes using min-sum density," in *Proc. 8th Int. Symp. Turbo Codes & Iter. Inform. Process. (ISTC)*, pp. 228–232, June 2014.
- [6] S.-Y. Chung, T. Richardson, and R. Urbanke, "Analysis of sum-product decoding of low-density parity-check codes using a Gaussian approximation," *IEEE Trans. Inform. Theory*, vol. 47, pp. 657–670, Feb. 2001.

- [7] P. Trifonov, "Efficient design and decoding of polar codes," *IEEE Trans. Commun.*, vol. 60, pp. 3221–3227, Nov. 2012.
- [8] D. Wu, Y. Li, and Y. Sun, "Construction and block error rate analysis of polar codes over AWGN channel based on Gaussian approximation," *IEEE Commun. Lett.*, vol. 18, pp. 1099–1102, July 2014.
- [9] H. Li and J. Yuan, "A practical construction method for polar codes in AWGN channels," in *Proc. IEEE 2013 Tencon - Spring*, pp. 223–226, Apr. 2013.
- [10] H. Vangala, E. Viterbo, and Y. Hong, "A comparative study of polar code constructions for the AWGN channel." available on arXiv:1501.02473v1 [sc.IT], Jan. 2015.
- [11] S. B. Korada, A. Montanari, E. Telatar, and R. Urbanke, "An empirical scaling law for polar codes," in *Proc. 2010 IEEE Int. Symp. Inform. Theory (ISIT)*, pp. 884–888, June 2010.
- [12] E. Arıkan, "A performance comparison of polar codes and Reed-Muller codes," *IEEE Commun. Lett.*, vol. 12, pp. 447–449, June 2008.
- [13] N. Hussami, S. B. Korada, and R. Urbanke, "Performance of polar codes for channel and source coding," in *Proc. 2009 IEEE Int. Symp. Inform. Theory (ISIT)*, 2009.
- [14] A. Eslami and H. Pishro-Nik, "On finite-length performance of polar codes: Stopping sets, error floor, and concatenated design," *IEEE Trans. Commun.*, vol. 61, pp. 919–929, Mar. 2013.
- [15] I. Tal and A. Vardy, "List decoding of polar codes," *IEEE Trans. Inform. Theory*, vol. 61, pp. 2213–2226, May 2015.
- [16] M. Qin, J. Guo, A. Bhatia, A. G. i. Fabregas, and P. H. Siegel, "Polar code constructions based on LLR evolution," *IEEE Commun. Lett.*, vol. 21, pp. 1221–1224, June 2017.
- [17] A. Elkelesh, M. Ebada, S. Cammerer, and S. ten Brink, "Decoder-tailored polar code design using the genetic algorithm," *IEEE Trans. Commun.*, vol. 67, pp. 4521–4534, July 2019.
- [18] J. Ha, J. Kim, and S. W. McLaughlin, "Rate-compatible puncturing of low-density parity-check codes," *IEEE Trans. Inform. Theory*, vol. 50, pp. 2824–2836, Nov. 2004.
- [19] B. P. Smith, A. Farhood, A. Hunt, F. R. Kschischang, and J. Lodge, "Staircase codes: FEC for 100 Gb/s OTN," *J. Lightw. Technol.*, vol. 30, pp. 110–117, Jan. 2012.
- [20] W. Coene, H. Pozidis, M. Van Dijk, J. Kahlman, R. Van Woudenberg, and B. Stek, "Channel coding and signal processing for optical recording systems beyond DVD," *IEEE Trans. Magnet.*, vol. 37, pp. 682–688, Mar. 2001.
- [21] M. Qiu, L. Yang, Y. Xie, and J. Yuan, "Terminated staircase codes for NAND flash memories," *IEEE Trans. Commun.*, vol. 66, pp. 5861–5875, Dec. 2018.
- [22] J. Hagenauer, E. Offer, and L. Papke, "Iterative decoding of binary block and convolutional codes," *IEEE Trans. Inform. Theory*, vol. 42, pp. 429–445, Mar. 1996.
- [23] P. Trifonov, "Randomized chained polar subcodes," in *Proc. 2018 IEEE Wireless Commun. Netw. Conf. Workshops (WCNCW)*, pp. 25–30, Apr. 2018.
- [24] J. Dai, K. Niu, Z. Si, C. Dong, and J. Lin, "Does Gaussian approximation work well for the long-length polar code construction?," *IEEE Access*, vol. 5, pp. 7950–7963, Jan. 2017.
- [25] B. Tahir and M. Rupp, "New construction and performance analysis of polar codes over AWGN channels," in *Proc. 24th Int. Conf. Telecommun. (ICT)*, pp. 1–4, May 2017.
- [26] M. Abramowitz and I. A. Stegun, eds., *Handbook of Mathematical Functions*. Dover, 1965.
- [27] A. Winkelbauer, "Moments and absolute moments of the normal distribution." available on arXiv:1209.4340v2 [math.ST], July 2014.
- [28] J. G. Proakis and M. Salehi, *Digital Communications*. McGraw-Hill, fifth ed., 2008.